

## POTENTIAL EFFECT OF BONE MARROW-DERIVED MESENCHYMAL STEM CELLS ON ZYMOGEN GRANULES AND RAB3D IN PAROTID SALIVARY GLANDS OF SENILE ALBINO RATS

Rabab Hassan\* and Amany A. Rabea\*\*

### ABSTRACT

**Background:** Age-related changes of salivary glands affect their functions and structure. Rab3D is localized to zymogen granules (ZGs) and plays a critical role in secretory granules maturation and exocytosis. Nowadays, application of life sciences is used in tissue regeneration.

**Objective:** The current study was designed to explore the possible effect of bone marrow-derived mesenchymal stem cells (BM-MSCs) on the function and morphology of ZGs in parotid glands of senile rats.

**Design:** Fourteen clinically healthy male albino rats were used. Seven adult rats aged 6-8 months were named as **Control adult (Group I)**. The remaining seven rats aged 18-20 months (old age). For each old age rat the parotid gland of the left side represented the **Old age untreated (Group II)** and injected by 0.2 ml phosphate buffered saline (PBS). While, the parotid gland of the right side represented the **Old age treated by stem cells (Group III)** and injected by  $1-1.5 \times 10^6$  BM-MSCs in 0.2 ml PBS. At the end of the experimental period (after four weeks), all the rats were euthanized and the parotid salivary glands were dissected out. The sections were prepared for histological, immunohistochemical and ultra-structural examinations in addition to real-time quantitative reverse transcription polymerase chain reaction (qRT-PCR) analysis. **Statistical analysis:** Data obtained from histomorphometric analysis and qRT-PCR assay were statistically described in terms of mean  $\pm$  standard deviation ( $\pm$  SD).

**Results:** Histological examination of Group I showed normal histological features of the terminal secretory units. Group II revealed that most of the acini were distorted and showed fatty degeneration. The oncocytes were noticeable. Group III illustrated more or less normal histological features. Immuno-expression of Rab3D was strong in Group I and Group III but mild in Group II. The ultra-structural examination of Group I showed apparently large and spherical ZGs. Group II revealed apparently small and ellipsoid ZGs. Lamellated lipofuscin granules were observed. Group III demonstrated obviously large and well defined spherical ZGs. The statistical results revealed that the highest means of Rab3D immunoreactivity area % and relative Rab3D gene expression level were demonstrated in Group I, followed by Group III, and the least values were for Group II.

**Conclusions:** Allogeneic BM-MSCs have positive effect on age-related changes of parotid salivary glands by restoring the terminal secretory units' structure, Rab3D expression as well as ZGs structure and function.

**KEY WORDS:** BM-MSCs, Aging, Zymogen granules, Rab3D, Parotid salivary gland.

\* Lecturer of Oral Biology, Faculty of Dentistry, Ain Shams University.

\*\* Associate Professor of Oral Biology, Faculty of Oral and Dental Medicine, Future University in Egypt.

## INTRODUCTION

The adult parotid gland is a pure serous exocrine salivary gland consists of serous acini, intercalated, striated, excretory and main ducts. In addition, connective tissue (C.T) stroma penetrates and divides the gland into lobes and lobules. The serous acini lay close to each other, separated by very scarce C.T and thin capillaries. The acinar cells are pyramidal in shape with rounded basal nuclei. Their cytoplasm is basophilic basally and eosinophilic apically. <sup>(1)</sup>

The acinar cells show spherical electron-dense membrane-bound zymogen granules (ZGs). These granules are less than 1mm in diameter and they are localized in the apical region of the cells. These granules have high calcium ions ( $\text{Ca}^{2+}$ ) content that makes them a physiological  $\text{Ca}^{2+}$  store in the acinar cells. ZGs contain 10 to 20 digestive enzymes such as amylase, ribonuclease (RNase) and deoxyribonuclease (DNase). Amylase is one of the most important endoenzymes in saliva. It influences individual oral perception, breaks down starch into maltose for digestion, and can affect overall nutritional status. <sup>(2,3)</sup>

The exocytosis of this digestive enzyme is induced by stimulation of both sympathetic and parasympathetic nervous systems. Amylase release involves budding of the secretory protein from endoplasmic reticulum (ER) then transporting to Golgi complex. The Golgi complex modifies and sorts the newly synthesized protein, then packs it into transport vesicles to be delivered to the ZGs. Afterwards, these ZGs move to the apical surface of the cell. Fusion between the secretory granule membrane, apical plasma membrane and neighboring granules membrane occurs. Consequently, exocytosis of the digestive enzyme into the apical lumen takes place. <sup>(4,5)</sup>

Ras superfamily is a protein superfamily of small guanosine triphosphate (GTP)-binding proteins. They are also called Ras superfamily of GTPases. This superfamily is characterized by the "G-domain" core. The GTP binding and hydrolysis

takes place in the "G domain" to form guanosine diphosphate (GDP). The Ras superfamily is divided according to structure and function into five main families: Ras, Rho, Ran, Rab and Arf GTPases. The GTPases belonging to the Rab family are important regulators of vesicular formation, transport and membrane fusion in eukaryotic cells. <sup>(6,7)</sup>

Parotid gland expresses four Rab3 isoforms (A, B, C and D). It is believed that, these proteins are essential in the control of intracellular membrane trafficking and regulated exocytosis. Rab3D is localized to ZGs and has been proposed as a critical factor in amylase release and in controlling the size of the secretory granules. <sup>(8)</sup>

Hypofunction of salivary glands either in form of hyposalivation or xerostomia can affect the quality of life due to impairment of lubrication, mastication, deglutition and increase of caries incidence as well as periodontitis. These function deteriorations may be related to diseases, radiotherapy for head and neck cancer, or age-related changes. These factors affect not only salivary gland functions but also the histological structure in which atrophied acinar cells and decreased cell numbers causing loss of functional parenchymal tissue. <sup>(9,10)</sup>

The current therapy of hyposalivation includes moisturizing dry oral tissues with artificial saliva and lubricating gel, or using drugs that increase the secretory function of the remaining acinar cells. <sup>(11)</sup> Unfortunately, these modalities only treat symptoms and provide a temporary relief. Moreover, the drugs used to treat hyposalivation cause well known multiple side effects such as excessive sweating, chills, dizziness, excessive tearing, flushing, voice change, stuffy nose, tremor, nervousness and diarrhea. <sup>(12)</sup>

Stem cell therapy for repair and functional restoration of the salivary glands could provide long-term and effective solution to damaged tissues induced by degenerative processes due to age-related changes or disease. <sup>(13)</sup>

Bone marrow-derived mesenchymal stem cells (BM-MSCs) show the ability to differentiate into

epithelial cells in vitro. They also show regenerative power to restore lost morphology as well as function by secreting bioactive factors. These factors create a repair environment through their antiapoptotic effects, immunoregulatory function and stimulation of endothelial progenitor cell proliferation that helps in vascularization of the damaged tissue. <sup>(14,15)</sup>

From this light, the current study was designed to explore the possible effect of BM-MSCs on the function and morphology of ZGs in parotid salivary glands of senile albino rats.

## MATERIALS AND METHODS

### Isolation and Culture of BM-MSCs

Two male albino rats 1.5 month old were used for isolation and culture of BM-MSCs at the Biochemistry and Microbiology Unit, Faculty of Medicine, Cairo University.

Bone marrow (BM) cells were flushed from tibia of the rats using Dulbecco's modified Eagle's medium (DMEM), supplemented with 10% fetal bovine serum (FBS) - purchased from (GIBCO™/ Bethesda Research Laboratories (BRL), Bethesda, Maryland, USA). In a biological safety cabinet, 35 ml of flushed BM cells were layered over 15ml Ficoll- Paque® density gradient medium (GIBCO™/Invitrogen, Grand Island, New York, USA), then centrifuged for 35 minutes at 400xg and the upper layer was discarded leaving mononuclear cell (MNC) layer at the interphase. This MNC layer was collected, washed twice in phosphate buffered saline (PBS) and centrifuged for 10 minutes at 200xg at 10°C. The isolated BM-MSCs were cultured and propagated on 25cm<sup>2</sup> culture flasks in complete culture medium consists of; cell culture medium Roswell Park Memorial Institute (RPMI)-1640 supplemented with 10% FBS and 1% penicillin-streptomycin, purchased from (GIBCO™/ BRL, Bethesda, Maryland, USA). The cells were incubated at 37°C in 5% humidified CO<sub>2</sub> incubator (Innova® CO-170, UK) for 7days upon formation of large colonies (80-90% confluence). The cultures

were washed twice with PBS and the cells were detached for 5 minutes at 37°C using 0.25% trypsin in 1millimole (mM) ethylenediaminetetraacetic acid (EDTA), (GIBCO™/ BRL, Bethesda, Maryland, USA).

The suspension then centrifuged at 2400 revolutions per minute (RPM) for 20 minutes. The cells were resuspended in serum-supplemented medium and incubated in 50cm<sup>2</sup> culture flask (Falcon®, Thermo Fisher Scientific, USA). The cultured cells were monitored using an inverted phase-contrast light microscope (Olympus®, Tokyo, Japan), at 200x magnification. The resulting cultures were referred to as first-passage cultures. The cells used for the experiment after the third passage. BM-MSCs in culture were characterized by their adhesiveness and fusiform shape. In addition, Florescent Analysis Cell Sorting (FACS) showed that these stem cells expressed CD90<sup>+</sup> marker but didn't express CD45<sup>+</sup> marker and this is specific to BM-MSCs. <sup>(16,17)</sup>

### Animals

Fourteen clinically healthy male albino rats were selected for this study. The rats were obtained from the animal house, Faculty of Medicine, Cairo University. The rats were numbered and housed in separate specially designed metal cages under controlled temperature, humidity and dark-light cycle, the rats were kept under good ventilation and allowed to have free access to tap water and adequate standard diet consisting of fresh vegetables and dried bread *ad-libitum*. This was done under supervision of specialized veterinarian.

After one week acclimatization period; seven adult rats were named as **Control adult (Group I)**: the rats of this group aged 6-8 months and weighing 200-250 gm.

The remaining seven rats were old age rats: 18-20 months and weighing 300-350 gm. For each old age rat the parotid gland of the left side represented the **Old age untreated (Group II)** and injected by 0.2 ml PBS. While, the parotid gland of the right

side represented the **Old age treated by stem cells (Group III)** and injected by  $1-1.5 \times 10^6$  BM-MSCs in 0.2 ml PBS and the cell numbers were calculated by the hemocytometer. <sup>(18)</sup>

### **Surgical procedures and injections**

The surgical procedures were performed under general anesthesia in which the old age rats received intramuscular injection of Xyla-Ject<sup>®</sup> (Phoenix<sup>™</sup> Pharmaceutical, Inc., USA) with a dose (10 mg/kg). <sup>(19)</sup>

After trimming the rat's hair, the trimmed area was disinfected by 10% povidone-iodine solution (Betadine<sup>®</sup> solution, Purdue Products L.P., England) and the open surgical technique was performed in which a small incision was done in front of the base of the external ear. <sup>(20)</sup> This technique allowed visualization of the parotid glands so that the injections were carried out under direct vision. For each gland, slowly intra-glandular injection with the previously mentioned dose was performed using 29 gauges (G) needles and 1ml syringes (Pic solution<sup>®</sup>, Artsana, Italy). The skin was sutured using sterile synthetic suture thread (Egysorb<sup>®</sup>2/0, 30mm, Taisier-Med., Egypt).

Post-operatively, local antibiotic (Bivatracin<sup>®</sup>, Aerosol powder Spray 150 ml, Egyptian Company for Advanced Pharmaceuticals (ECAP), Egypt), was applied 3times/day/rat for 3days. <sup>(21)</sup> Also, Cefotaxime antibiotic (Cefotax 500mg<sup>®</sup>, Egyptian Int. Pharmaceutical Industries CO. (E.I.P.I.CO.), Egypt) was administrated via intraperitoneal (I.P) injection with dose 67.5 mg/kg/day for 3 days. <sup>(22)</sup> Analgesics were administered immediately following the surgery in which diclofenac potassium (Cataflam-75mg<sup>®</sup>, Novartis, Switzerland) was administrated via I.P injection with dose 10 mg/kg/day for 3 days. <sup>(23)</sup>

### **Animals sacrifice**

Four weeks post-operatively, the animals in all groups were euthanized using ketamine over dose. <sup>(24)</sup>

### **Parotid gland extraction**

From each numbered rat, the parotid salivary glands of the right and left sides were dissected out. Each gland was dissected free of the surrounding lymph nodes and fat. Each gland was split into three portions and placed in three plain vacutainers (Voma Med<sup>®</sup> 5ml, Turkey) numbered according to the rat's number and labeled either right or left side, in order to be able to compare the results of different examination methods of the same rat. One portion of the gland was fixed immediately in 10% neutral buffered formalin solution to be prepared for histological staining and immunolabeling. <sup>(24)</sup> The second portion was sliced into 1mm<sup>3</sup> cubes and fixed in 2.5% glutaraldehyde buffered with 0.1mole (M) phosphate buffer at pH 7.4, for 2 hours at 4°C to be examined by transmission electron microscope (TEM). <sup>(25)</sup> The third portion was immediately frozen in liquid nitrogen and stored at -80°C for real-time quantitative reverse transcription polymerase chain reaction (qRT-PCR) analysis. <sup>(26)</sup>

### **Specimen preparation**

After immediate fixation of the gland portions in 10% neutral buffered formalin solution as previously mentioned, the specimens were left in the fixative for 48 hours. Then they were washed by tap water, dehydrated in ascending grades of ethyl alcohol, cleared in xylene and embedded in paraffin wax. <sup>(24)</sup> Two sets of sections were prepared. One set was prepared for hematoxylin and eosin (H&E) staining. The other set was prepared for immunolocalization or labeling of Rab3D.

### **H&E staining**

A set of serial 4-5µm thickness sections was obtained and mounted on clean glass slides. Afterwards the tissue sections were deparaffinized in xylene and rehydrated by ethanol series ending with pure H<sub>2</sub>O (Millipore Corporation, Temecula, CA, USA) before histological staining using H&E solutions (Sigma, St. Louis, MO, USA), to explore the histological details of the terminal secretory units. <sup>(24)</sup>

### Immunohistochemistry

Immunolocalization or labeling of Rab3D was carried out on the other set of paraffin sections of 4-5 $\mu$ m in thickness mounted on positively charged microscope slides. The sections were incubated for 2 hours in hot oven at 56°C then, deparaffinized in xylene and rehydrated by ethanol series ending with pure H<sub>2</sub>O (Millipore Corporation, Temecula, CA, USA). After washing the slides with PBS, unmasking of the antigens was performed as the sections were incubated in 0.05 mg/ml proteinase K in 0.05 M Tris-HCl, 0.01M EDTA and 0.01M NaCl, pH 7.8 for 10 minutes at 37°C. After two washes with PBS, unmasking of the antigens was completed using antigen retrieval citrate buffer solution for 10 minutes in boiling water. The sections were treated for 5 minutes with 3% hydrogen peroxide to inhibit endogenous peroxidase activity. The slides were incubated with normal rabbit serum for 20 minutes to reduce non-specific reactions. The sections were then incubated with the primary antibody overnight in a humidified chamber at 4°C. The primary antibody used was anti-Rab3D polyclonal antibody (Invitrogen®, Thermo Fisher, USA) with dilution 1:100. In the next day, after washing in PBS, the slides were incubated with secondary universal antibody (Vectastain Universal Elite ABC-peroxidase kit, Vector Laboratories) and then incubated with the Avidin-Biotin complex (ABC) (Vectastain Universal Elite ABC kit, Vector Laboratories, Burlingame, CA, USA) according to the manufacturer's protocol. Afterwards, 3,3'-diaminobenzidine (DAB) was applied for the same amount of time on all labeled sections until development of the desired brown color. At last, the sections were counter-stained with Mayer's hematoxylin (Sigma, St. Louis, MO, USA) for 30 seconds to visualize the tissue topography. The negative control was obtained by omitting the primary antibody from the protocol outlined above. <sup>(27)</sup>

Histological and immunohistochemical examinations were carried out using light microscope (Olympus® BX 60, Tokyo, Japan) and the terminal secretory units were photographed at 400x magnification.

### Preparation for TEM

After fixation of the gland portions (1mm<sup>3</sup>) in 2.5% glutaraldehyde buffered with 0.1M phosphate buffer at pH 7.4 and 4°C for 2 hours as previously mentioned, they were post fixed in 1% osmium tetroxide in the same buffer at 4°C for 1 hour. Then, the specimens were dehydrated and embedded in epoxy resin in flat capsules and polymerized for 24 hours at 60°C. Ultrathin sections were obtained using ultra-microtomy (Lecia Ultra-Cut®, UK). The ultra-thin sections were then collected on copper grids and stained with uranyl acetate and lead citrate. <sup>(25)</sup> The sections were examined for ZGs and photographed at 40,000x magnification using TEM (JEOL JEM® 1010 transmission electron microscope, Jeol Ltd, Tokyo, Japan) at Regional Center of Mycology and Biotechnology (RCMB), Al-Azhar University, Egypt.

### qRT-PCR Detection of Rab3D gene expression

The qRT-PCR for cloning and sequencing of Rab3D fragments was performed at Biochemistry and Microbiology Unit, Faculty of Medicine, Cairo University.

After immediate freezing of the third portion of the gland in liquid nitrogen and storing it at -80°C as previously mentioned, total ribonucleic acid (RNA) was extracted from each frozen sample using RN easy Purification Reagent (Qiagen®, Valencia, CA, USA), according to manufacturer's instructions. Then, a sample of isolated total RNA (1 $\mu$ g) was reverse transcribed to be converted into complementary deoxyribonucleic acid (cDNA) using Moloney-murine leukemia virus (M-MLV) reverse transcriptase (RT) (Promega®, Madison, USA), in the presence of rat Rab3D primer (165 bp), (Applied Biosystems®, Foster City, CA, USA). To quantify relative amplicon amounts of Rab3D, SYBR® Green PCR Master Mix fluorescent (Applied Biosystems®, Foster City, CA, USA) was used in a final volume of 10 microliters ( $\mu$ l).

The qRT-PCR was performed using Step One Plus® Real-Time PCR System (Applied Biosystems®, Foster City, CA, USA).

The PCR was performed for repeated 35 cycles. Each cycle consisted of:

- Denaturation at 95°C for 15 seconds.
- Annealing at 55 °C to 63 °C for 15 seconds.
- Elongation at 72 °C for 15 seconds.

After completion of the 35<sup>th</sup> cycle, the elongation step was continued for additional 10 minutes at 72°C. Beta-actin ( $\beta$ -actin) gene was used as an invariant endogenous housekeeping gene (reference gene). So, the  $\beta$ -actin cDNA primer (202 bp) was used (Applied Biosystems®, Foster City, CA, USA). The sequences of PCR primer pairs used for each gene are shown in table 1. Control PCR reactions lacking first-strand cDNA or RT were appropriately negative.

The resulting PCR products were separated by electrophoresis in 1% agarose gel (TA cloning kit®, Invitrogen, Grand Island, New York, USA), stained with ethidium bromide (TA cloning kit®, Invitrogen, Grand Island, New York, USA), visualized and photographed under ultraviolet light using spectrophotometry (dual wave length Beckman®, Spectrophotometer, USA). Data were analyzed using the ABI Prism® Sequence Detection System Software (Pimer Express®, Applied Biosystems, Foster City, CA, USA) and quantified using the v1.7 Pimer Express® Software (Applied Biosystems, Foster City, CA, USA).<sup>(26)</sup>

Relative expression of studied genes was calculated using the comparative threshold cycle method after normalization to the  $\beta$ -actin. The relative quantification (RQ) was calculated according to the following equation.<sup>(28)</sup>

1.  $\Delta Ct = Ct_{\text{assessed gene}} - Ct_{\text{reference gene}}$
2.  $\Delta \Delta Ct = \Delta Ct_{\text{sample}} - Ct_{\text{control gene}}$
3.  $RQ = 2^{-(\Delta \Delta Ct)}$

TABLE (1): Showing the sequence of the primers used for qRT-PCR.

	Primer sequence
<b>Rab3D</b>	Forward primer: 5'-TCGCTCACCTCCTATTCTAG-3' Reverse primer: 5'-TGTTTAACAGGGCCACTGAG-3'
<b><math>\beta</math>-actin</b>	Forward primer: 5'-TATCCTGGCCTCACTGTCCA -3' Reverse primer: 5'-AACGCAGCTCAGTAACAGTC-3'

### Histomorphometric analysis

For measuring the optical density of the immunolabeling, the immunolabeled sections were examined using an image analyzer computer system. The image analyzer computer system consisted of a color video camera, color monitor, hard disc of IBM personal computer connected to the microscope and controlled by Leica Qwin 500 software (LEICA® Imaging Systems Ltd, Cambridge, England). At first the image analyzer was calibrated automatically to convert the measurement units from pixels which were produced by the image analyzer program into actual micrometer ( $\mu\text{m}$ ) units.

The image analysis system was used to assess the area percentage (area %) of Rab3D immunoreactivity in the studied specimens. The intensity of the reaction within the cells was determined by measuring the optical density in 10 fields in each section under a power of 400x magnification. After grey calibration, the image was transformed into a grey delineated image to choose the areas exhibiting positive reaction with accumulation of all grades of reactivity (minimum, maximum and median grey). Afterwards, the areas of positive reaction were masked by a blue binary color. Finally, the mean values were calculated for each specimen. All calculations of the area % were carried out in relation to a standard measuring frame of an area 118476.6 $\mu\text{m}^2$ .

### Statistical analysis

All the data obtained from histomorphometric analysis and qRT-PCR assay were statistically assessed and described in terms of mean values  $\pm$  standard deviation ( $\pm$  SD). The One-way Analysis of Variance (ANOVA) test was used to compare between the studied groups. When ANOVA test showed statistically significant result it was followed by the Honest Significant Difference (HSD) Tukey's post hoc test. The probability value (P-value)  $<0.001$  was considered as highly significant and P-value  $\leq 0.05$  was considered as significant. The statistical analysis was performed using the software Statistical Package for the Social Science (SPSS® Inc., Chicago, IL, USA) version 20 for Microsoft® Excel 2013 window (Microsoft® Corporation, NY, USA).

## RESULTS

### Histological results

#### *Group I (Control adult)*

Histological examination of Group I showed that the glands were divided by C.T septa into lobes and lobules. Normal histological features of terminal secretory units were noticed. The terminal secretory units of the parotid glands were formed of serous acini. The acini were almost spherical in shape. Each acinus was composed of pyramidal cells. The apices of the cells were eosinophilic and directed toward an apparently narrow lumen. The acinar cells showed moderately basophilic cytoplasm. Apparently large, spherical and basally situated nuclei were noticed. The flattened nuclei of myoepithelial cells were demonstrated around some acini (**Fig. 1a**).

#### *Group II (Old age untreated)*

Histological examination of Group II revealed apparent shrinkage in overall size of the acini. Apparent decrease in acini number was observed.

Most of the acini were distorted and most of the acinar cells showed ill-defined outline. The acinar cells showed; cytoplasmic vacuolation, many pyknotic nuclei and nuclei with marginated chromatin. The apices of the cells were vacuolated and mildly eosinophilic. The flattened nuclei of myoepithelial cells could be detected around few acini. The oncocytes were noticeable. Fatty degeneration of the acini and C.T stroma was obvious in this group. The C.T septa showed inflammatory cells infiltration (**Fig. 1b**).

#### *Group III (Old age treated by stem cells)*

Histological examination of Group III illustrated more or less normal histological features. The C.T septa divided the gland into lobes and lobules. The acini shape was nearly spherical. The acinar cells were pyramidal with their apices directed toward an apparently narrow lumen. Most of the cells' apices were eosinophilic. The acinar cells exhibited moderately basophilic cytoplasm. Spherical, apparently large and basally situated nuclei were noticed. However few pyknotic nuclei could be detected. The myoepithelial cells' flattened nuclei were observed around some acini (**Fig. 1c**).

### Immunohistochemical results

Different patterns of nuclear and cytoplasmic immunoreactivity for anti-Rab3D antibody were detected in the acinar cells of the studied groups. Group I revealed strong nuclear and cytoplasmic immunoreactivity for anti-Rab3D antibody (**Fig. 2a**). On the other hand, Group II exhibited negative nuclear immuno-expression of Rab3D. Mild cytoplasmic immuno-expression was detected in some acini, while others showed negative cytoplasmic immuno-expression (**Fig. 2b**). However, Group III demonstrated strong nuclear and cytoplasmic immuno-expressions of Rab3D (**Fig. 2c**).

### Electron microscopic results

Group I showed apparently large, variable sized, spherical and highly electron-dense ZGs with well defined boundaries. The ZGs were granular in appearance. Highly electron-dense membrane delineating the granules could be noticed (**Fig. 3a**). Group II revealed apparently small, variable sized and mildly electron-dense ZGs. Few granules were spherical while many had ellipsoid profile. Few granules had well defined borders, but many granules lacked a definite boundary. The ZGs were granular in appearance. Only few granules showed

the limiting granule membrane that appeared mildly electron-dense. Apparently variable sized and shaped membrane-bounded lipofuscin granules could be detected. The lipofuscin granules were lamellated with electron-dense and electron-lucent lamellae. lipofuscin granules were surrounded by moderately electron-dense membrane (**Fig. 3b**). Group III demonstrated obviously large, variable sized and well defined spherical ZGs. Some ZGs were highly electron-dense while others showed moderate electron-density. The ZGs appeared granular and bounded by highly electron-dense membrane (**Fig. 3c**).

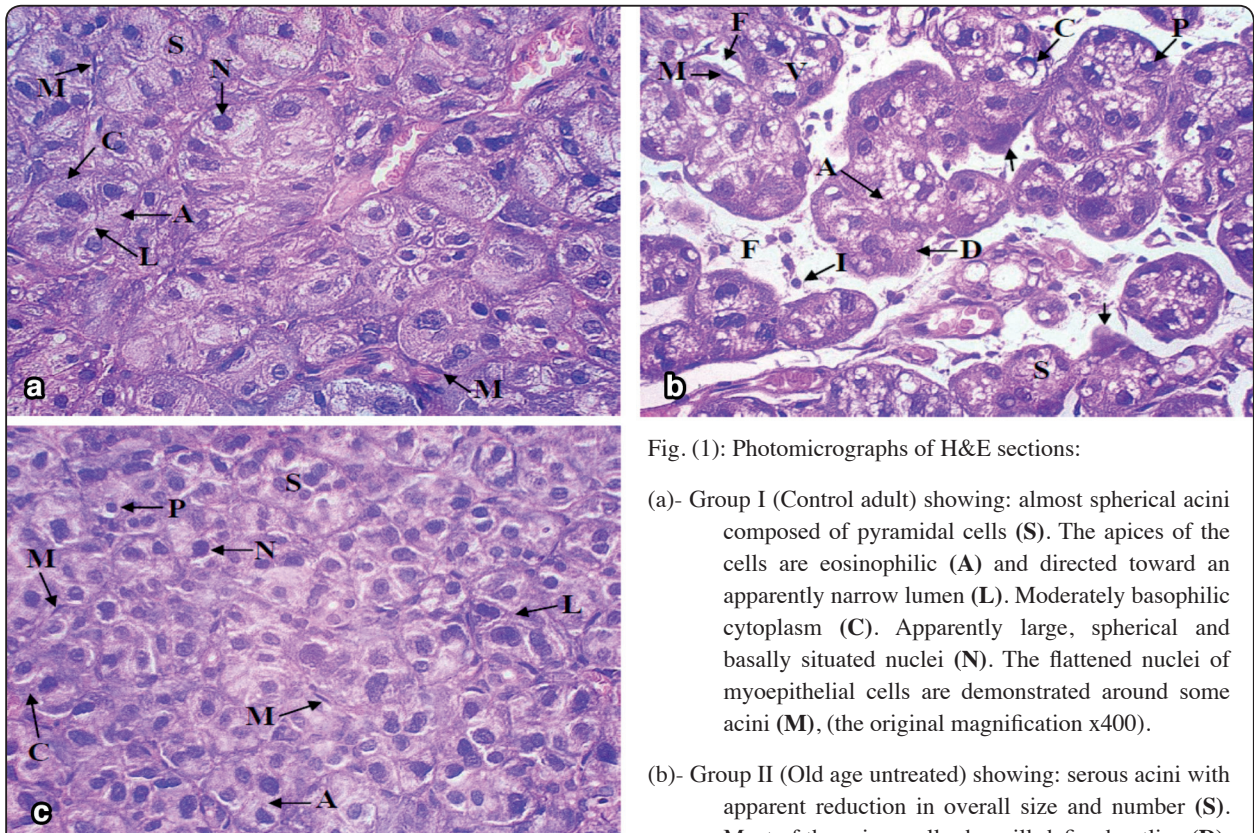


Fig. (1): Photomicrographs of H&E sections:

(a)- Group I (Control adult) showing: almost spherical acini composed of pyramidal cells (S). The apices of the cells are eosinophilic (A) and directed toward an apparently narrow lumen (L). Moderately basophilic cytoplasm (C). Apparently large, spherical and basally situated nuclei (N). The flattened nuclei of myoepithelial cells are demonstrated around some acini (M), (the original magnification x400).

(b)- Group II (Old age untreated) showing: serous acini with apparent reduction in overall size and number (S). Most of the acinar cells show ill-defined outline (D). Cytoplasmic vacuolation (V). Pyknotic nuclei (P). Nuclei with marginated chromatin (C). The apices of the cells are vacuolated and mildly eosinophilic (A). The flattened nuclei of myoepithelial cells are detected around few acini (M). The oncocytes (arrows). Fatty degeneration (F). Inflammatory cells infiltration (I), (the original magnification x400).

(c)- Group III (Old age treated by stem cells) showing: nearly spherical acini (S). The acinar cells are pyramidal with their apices directed toward an apparently narrow lumen (L). Most of the cells' apices are eosinophilic (A). Moderately basophilic cytoplasm (C). Spherical, apparently large and basally situated nuclei (N). Few pyknotic nuclei (P). The myoepithelial cells' flattened nuclei are observed around some acini (M), (the original magnification x400).

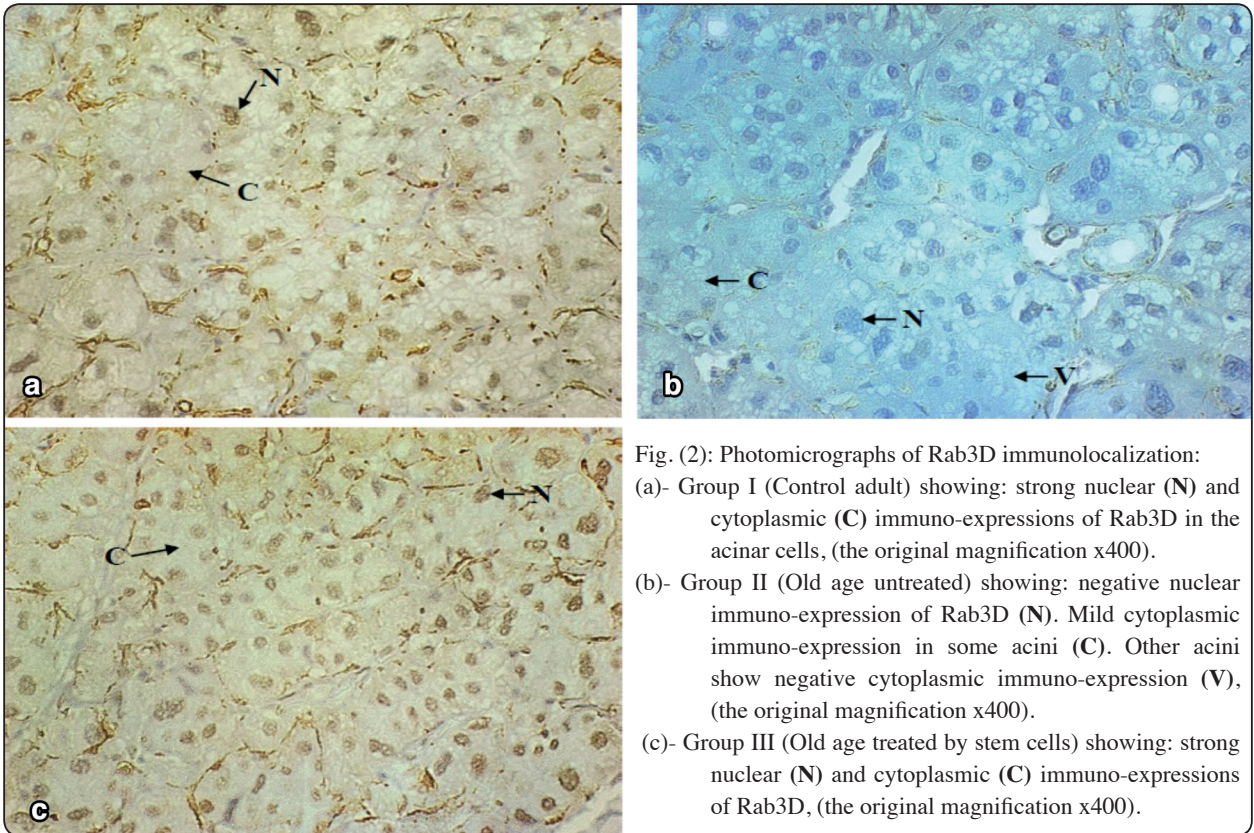


Fig. (2): Photomicrographs of Rab3D immunolocalization: (a)- Group I (Control adult) showing: strong nuclear (N) and cytoplasmic (C) immuno-expressions of Rab3D in the acinar cells, (the original magnification x400). (b)- Group II (Old age untreated) showing: negative nuclear immuno-expression of Rab3D (N). Mild cytoplasmic immuno-expression in some acini (C). Other acini show negative cytoplasmic immuno-expression (V), (the original magnification x400). (c)- Group III (Old age treated by stem cells) showing: strong nuclear (N) and cytoplasmic (C) immuno-expressions of Rab3D, (the original magnification x400).

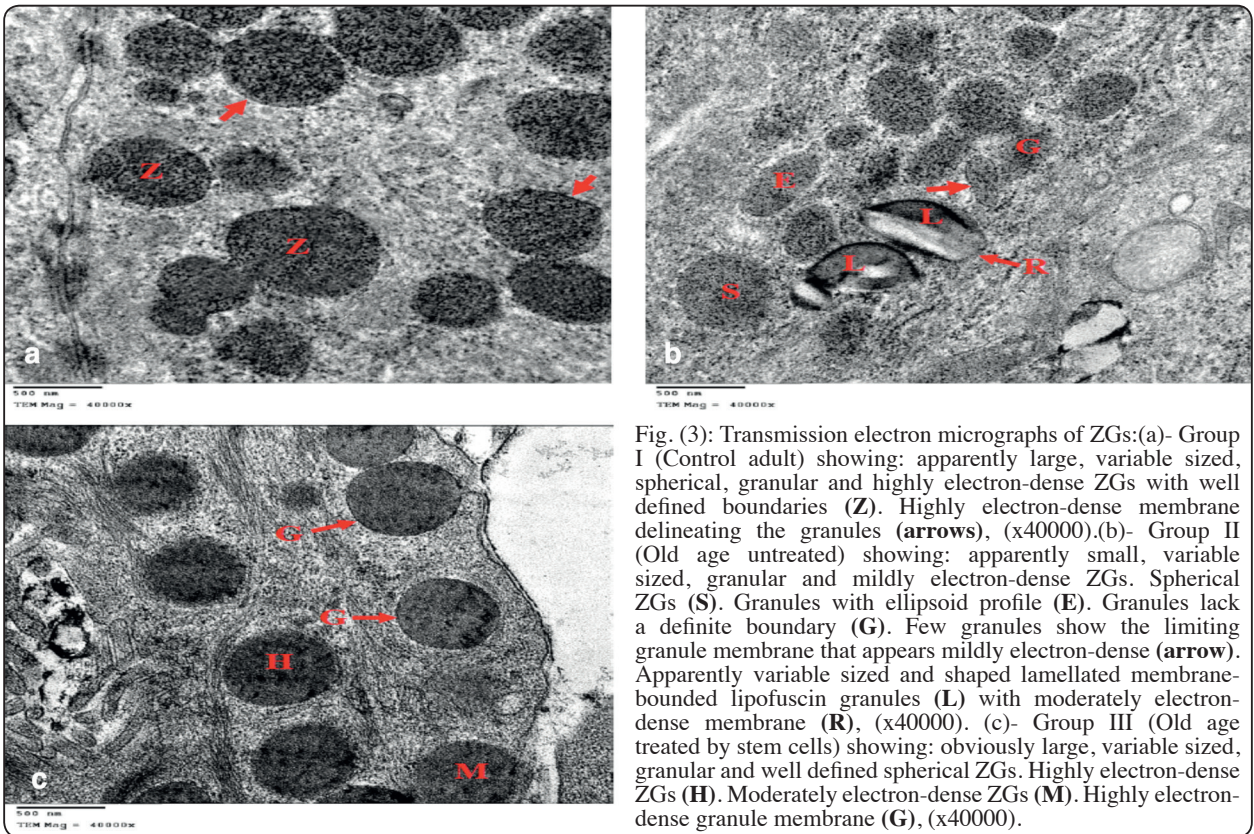


Fig. (3): Transmission electron micrographs of ZGs:(a)- Group I (Control adult) showing: apparently large, variable sized, spherical, granular and highly electron-dense ZGs with well defined boundaries (Z). Highly electron-dense membrane delineating the granules (arrows), (x40000).(b)- Group II (Old age untreated) showing: apparently small, variable sized, granular and mildly electron-dense ZGs. Spherical ZGs (S). Granules with ellipsoid profile (E). Granules lack a definite boundary (G). Few granules show the limiting granule membrane that appears mildly electron-dense (arrow). Apparently variable sized and shaped lamellated membrane-bounded lipofuscin granules (L) with moderately electron-dense membrane (R), (x40000). (c)- Group III (Old age treated by stem cells) showing: obviously large, variable sized, granular and well defined spherical ZGs. Highly electron-dense ZGs (H). Moderately electron-dense ZGs (M). Highly electron-dense granule membrane (G), (x40000).

**Statistical results**

**a) Rab3D immunoreactivity area %**

Group I showed the highest mean area % of Rab3D immunoreactivity followed by Group III,

and the least value was for Group II. One-way ANOVA showed highly significant difference between the studied groups. Tukey's post hoc test showed significant difference between each group when compared with the others (table 2 & fig. 4).

TABLE (2): Showing the mean ± SD values, the range values, results of ANOVA as well as Tukey's post hoc tests for the comparison between the studied groups regarding Rab3D immunoreactivity area %.

Rab3D immunoreactivity area %	Group I (Control adult)	Group II (Old age untreated)	Group III (Old age treated by stem cells)	ANOVA	p-value
Mean±SD	79.76±0.09 <sup>a</sup>	10.95±0.08 <sup>b</sup>	77.76±0.12 <sup>c</sup>	2057.912	<0.001**
Range	79.67-79.89	10.8-11.03	77.62-77.92		

*Different superscript letters in the same row indicate significant difference between each group when compared with the others according to Tukey's post hoc test. \*\*: Highly significant at p-value <0.001.*

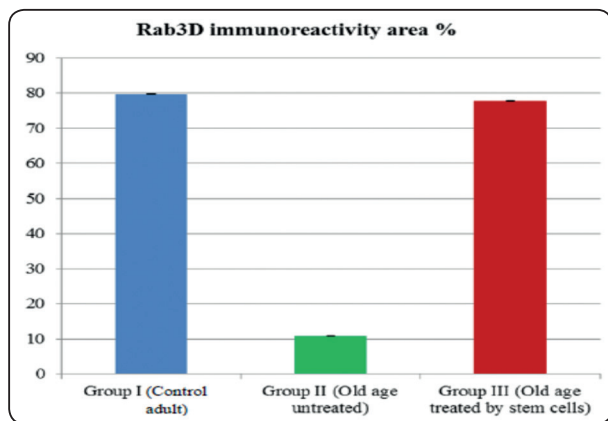


Fig. (4): Bar chart representing mean and SD values of Rab3D immunoreactivity area % in the studied groups.

**b) qRT-PCR assay**

Group I showed the highest mean of relative Rab3D gene expression level followed by Group III, and the least value was for Group II. Values were normalized to β-actin gene expression. One-way ANOVA showed highly significant difference between the studied groups. Tukey's post hoc test showed significant difference between each group when compared with the others (table 3 & fig. 5).

TABLE (3): Showing the mean ± SD values, the range values, results of ANOVA as well as Tukey's post hoc tests for the comparison between the studied groups regarding relative Rab3D gene expression levels.

qRT-PCR of Rab3D	Group I (Control adult)	Group II (Old age untreated)	Group III (Old age treated by stem cells)	ANOVA	p-value
Mean±SD	1.00±0.01 <sup>a</sup>	0.23±0.14 <sup>b</sup>	0.81±0.06 <sup>c</sup>	274.743	<0.001**
Range	1-1.01	0.11-0.43	0.75-0.88		

*Different superscript letters in the same row indicate significant difference between each group when compared with the others according to Tukey's post hoc test. \*\*: Highly significant at p-value <0.001.*

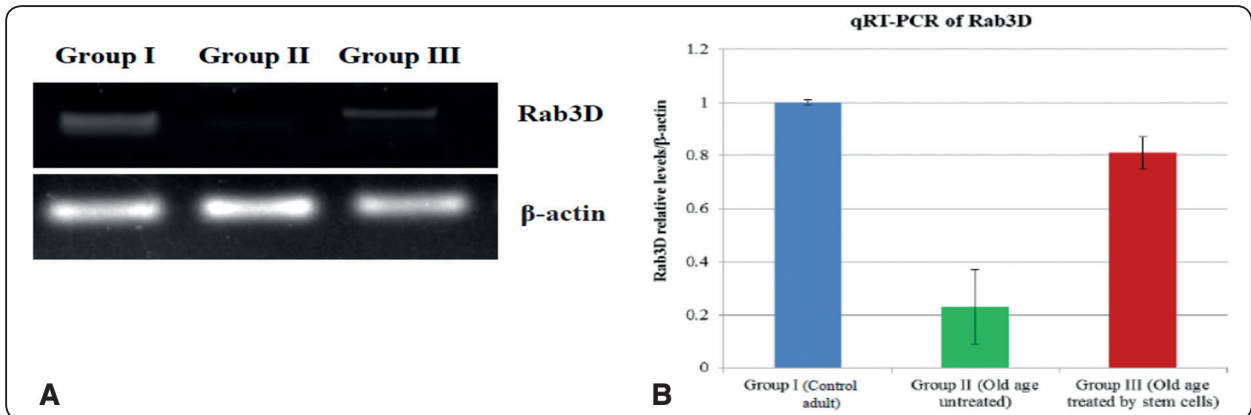


Fig. (5): (A) Results of qRT-PCR of Rab3D in the studied groups. (B) Bar chart representing mean and SD values of relative Rab3D gene expression levels in the studied groups. Values were normalized to  $\beta$ -actin gene expression.

## DISCUSSION

Aging is a continuous, slow dynamic and complex process that has harmful impact due to increased oxidative stress which induces accumulation of damaged mitochondria, inflammation, hormonal changes and formation of reactive oxygen species (ROS) that cause damage to molecular structures such as lipids, proteins, enzymes and DNA which appear gradually in old age in form of system disorders and organ dysfunctions. <sup>(29-31)</sup>

The parotid gland was the gland of choice in the present study since when it is stimulated; parotid contributes with more than 50% of the total salivary secretion. Furthermore, during aging the parotid gland can be more subjected to oxidative damage via ROS by presenting a predominantly aerobic metabolism. <sup>(32,33)</sup>

Rab3D is predominantly localized in salivary glands and it is responsible for maturation of secretory granules and regulation of protein exocytosis. <sup>(34,35)</sup> Moreover, a study was conducted by **Rajaniello et al., (1999)** <sup>(36)</sup> to determine Rab3 isoforms expressed mostly in rat's parotid gland using qRT-PCR assay. The authors' results indicated that Rab3D is the major Rab3 isoform expressed in parotid gland.

Nowadays, application of life sciences and materials engineering such as combination of cells, biomaterials, and biochemicals is used to develop

and recreate natural organ environment that helps in tissue regeneration. <sup>(37)</sup>

In this study, allogeneic BM-MSCs were used as treatment for parotid gland during aging, because MSCs are multipotent stem cells. They are able to differentiate into many cell types, such as acinar cells, and salivary epithelial cells. <sup>(38)</sup> Also MSCs exhibit low levels of major histocompatibility complex (MHC) class I expression and there is no expression of either MHC class II markers or costimulatory molecules, which are necessary for full activation of T cells that leads to stem cells transplant rejection. During aging the autologous MSCs exhibit impaired functional properties. Therefore, allogeneic MSCs could be more effective than the use of dysfunctional autologous MSCs. <sup>(39)</sup>

In the current study, histological examination of parotid glands in Group I showed normal histological features of the terminal secretory units. The secretory units were formed of serous acini. The acini were almost spherical in shape and composed of pyramidal cells. These findings are in accordance with those of **Pringle et al., (2013)** <sup>(40)</sup> who found that the serous acinar cells have pyramidal shape and are joined together to form spherical shapes; the secretory units. The ultra-structure examination of the same group showed spherical, highly electron-dense and granular ZGs with well defined boundaries. These findings are in parallel with those of

**Mednieks et al., (2009)** <sup>(41)</sup> who described these features as the mature form of ZGS.

In the present study, histological examination of parotid glands in all studied groups revealed the presence of flattened nuclei of myoepithelial cells around some acini. This result is in parallel with that of **Tamgadge et al., (2013)** <sup>(42)</sup> who noticed in routine histological preparations that, myoepithelial cells are indistinct and only their nuclei which are situated between the parenchymal cells and their basement membrane could be determined by the light microscope. The myoepithelial cells have contractile function that helps in eviction of saliva and preventing the damage of neighboring cells through this process. <sup>(43)</sup>

On the contrary, histological examination of parotid glands in Group II showed apparent shrinkage in overall size of the acini and decrease in acini number. Most of the acini were distorted and most of acinar cells showed ill-defined outline. The acinar cells showed; cytoplasmic vacuolation, many pyknotic nuclei and nuclei with marginated chromatin. Also, inflammatory cells infiltration was observed in the C.T septa. All these findings are coinciding with those of **Chakrabarti et al., (2012)** and **Yasear et al., (2013)** <sup>(44, 45)</sup> who reported morphological and histological changes in aged rabbit's parotid, submandibular and minor salivary glands. These changes include atrophy, epithelial degeneration, loss of acini, localized areas of nuclear pyknosis in the parenchyma, fibrosis, and inflammatory cells infiltration. The authors stated that these changes are considered as a sign of degenerative ageing process, due to generated oxidative stress that causes reduced cellular proliferation and increased apoptosis which may be designed as aging stress response pathway. <sup>(46, 47)</sup>

In herein study, oncocytes were noticeable in Group II. **Kontaxis et al., (2004)** <sup>(48)</sup> reported incidental appearance of solitary oncocytes in aged salivary tissue. The authors attributed this finding to the fact that during aging, mitochondrial

enzymes exhibit diminished function that results in compensatory hyperplasia of the mitochondria and consequently oncocytic change. The changes in the mitochondria could be explained also according to **Terman et al., (2010)** <sup>(49)</sup> who stated that, the mitochondria are major targets of ROS attack which causes obvious abnormal structural changes in mitochondria with age ranging from swelling, mitochondrial enlargement (giant mitochondria) with insufficient functions, loss of cristae, up to complete destruction of the inner membrane.

Histological examination of Group II in the present study revealed fatty degeneration of the acini and C.T stroma. Moreover, the ultra-structure examination of the same group demonstrated apparently small, variable sized, granular and mildly electron-dense ZGs with different profiles. Most of the granules lacked a definite limiting granule membrane. Furthermore, apparently variable sized and shaped lamellated membrane-bounded lipofuscin granules were noticed. These results are in agreement with those of **Hagras et al., (2011)** and **Tirapelli et al., (2012)** <sup>(50, 51)</sup> who reported degenerated secretory granules, accumulation of lipofuscin granules, and lipid droplets in parotid gland of old age albino rats. The reported changes in ZGs could be attributed to the fact that ZGs membrane is formed of many proteins among which are Rab3D as well as secretory carrier membrane proteins (SCAMPs) which are linked by lipid microdomains. These granule membrane proteins play an important role in membrane trafficking and exocytosis. <sup>(52)</sup> ROS attack the granule membrane proteins and lipids leading to damage of the membrane. <sup>(30)</sup> Moreover, ROS react to proteins and nucleic acids in the ZGs leading to impairment in ZGs stability. <sup>(53)</sup> Therefore, these changes in the ZGs lead to the reduced level of cellular secretory activity in the gland of old rats. <sup>(25)</sup> The fatty degeneration and presence of lipofuscin granules in our study could be related to lipid peroxidation process due to increased ROS production that results from declined ATP production by the aged

mitochondria.<sup>(49)</sup> However, the origin of lipid in lipofuscin granules is still unknown but it is suggested to be due to transformation of Golgi complexes and mitochondria.<sup>(25)</sup>

Histological and ultra-structure results of Group III in our study were more or less comparable to those of the control adult group. As previously mentioned, there is increased oxidative stress during aging which induces many changes including inflammation and formation of ROS that cause damage to molecular structures such as lipids, proteins, enzymes and DNA.<sup>(29-31)</sup> So, based on the previously mentioned fact, our results of group III could be explained according to **Xu et al., (2012)**<sup>(54)</sup> who stated that the salivary flow rate in mice with Sjogren's syndrome like autoimmune disease was restored after treatment with MSCs due to their anti-inflammatory effect. Moreover, it was reported that in irradiated mice, their salivary glands suffering from ROS generated by ionizing radiation when treated by MSCs, they displayed increased blood supply, significant reduction in cell apoptosis, and high regeneration of acinar cells. These findings are related to the vasculogenic and paracrine effects of the MSCs that can restore the gland functions.<sup>(55,56)</sup> Furthermore, after stem cells transplantation in damaged tissues or organs, they become influenced by several factors such as inflammatory cytokines which have different functions. Inflammatory cytokines activate many cell processes by acting as growth factors and thus enhance the MSCs function in reconstruction of the damaged cells and tissues.<sup>(57,58)</sup> On top, the improvement recorded in this study after treatment by BM-MSCs could be explained according to **Liu et al., (2017)**<sup>(59)</sup> who reported that the BM-MSCs exhibit potent antioxidant effects that provide protection against aging-induced oxidative stress. It is worthy to mention that, the absence of fatty degeneration and lipofuscin granules from Group III in the current study could be related to the antioxidant effect of BM-MSCs that attenuates the lipid peroxidation process.<sup>(60)</sup> Also, BM-MSCs enhance the function of

Rab3D.<sup>(61)</sup> This enhanced Rab3D function plays a supportive role in the removal of ROS by-products such as lipofuscin.<sup>(62,63)</sup> This could be attributed to the pleiotropic role that Rab3D plays in removing ROS and preventing their production as well as modifying the lipid composition of lipofuscin granules. Consequently Rab3D directs cellular response towards the oxidative stress.<sup>(64,65)</sup>

In the current study, the immunohistochemical results of Group I revealed strong nuclear and cytoplasmic immuno-expressions of Rab3D. Our results are in agreement with those of **Rajaniello et al., (1999)**<sup>(36)</sup> who reported that in parotid acinar cells, Rab3D is localized to ZGs membranes and cytosolic. Moreover, our qRT-PCR results of the same group are in agreement with those of **Rajaniello et al., (1999)**<sup>(36)</sup> who noticed using the qRT-PCR assay that Rab3D gene is highly expressed in the parotid gland. Rab3D is active when it binds to GTP. The localization of active Rab3D to the ZGs membranes starts since the active Rab3D moves from the cytoplasm to the developing secretory vesicle at the inner nuclear membrane and becomes in association with the vesicle membrane. This enables Rab3D to perform its function in maturation of secretory granules and regulation of protein exocytosis.<sup>(64,66,67)</sup> It should be mentioned that the central role that Rab3D plays from granule biogenesis up to the exocytosis, is mediated through the modulation of the granule proteins, and modification of lipids present in the membranes of the granules, organelles as well as those of the cell membrane throughout the secretory pathway. The modification of membranes lipids clarifies the role of these lipids in the formation of exocytotic sites.<sup>(64)</sup>

The immunohistochemical, qRT-PCR and statistical results of Group II in the present study revealed decreased expression of Rab3D. Our results are in agreement with those of **Batista et al., (2012)**<sup>(68)</sup> who reported reduced expression of Rab3D at both the mRNA and protein levels in lacrimal glands of the aging rats. The authors related these changes to the aging-induced oxidative stress that

leads to accumulation of advanced glycation end products (AGEs) which have damaging potential as they contribute to the generation of ROS. The ROS cause DNA damage and lead to formation of dominant-negative Rab3D mutants. The mutant Rab3D is not only unable to bind to the granule membrane but also has inhibitory effect on secretion. Moreover, inhibition of secretion does not require binding of mutant Rab3D to the granule membrane because mutant Rab3D inhibits the secretion by interacting with other essential regulating proteins. <sup>(66,69)</sup>

The immunohistochemical, qRT-PCR and statistical results of Group III in the present study almost resembled those of Group I. This could be explained according to the fact that BM-MSCs have anti-inflammatory effect, secrete paracrine factors and reduce ROS levels. <sup>(70)</sup> Therefore, BM-MSCs enhance the expression of active Rab3D that leads to improved secretory function of the gland. <sup>(61)</sup>

To sum up, aging is a complicated process that has harmful impact on the structure of the terminal secretory units in parotid salivary glands. Also, aging affects the terminal secretory units' function by affecting the ZGs and their related Rab3D.

Allogeneic BM-MSCs have positive effect in restoring the terminal secretory units' structure. Also they have supportive role in restoring the ZGs structure and function through enhancing the expression of Rab3D.

## REFERENCES

- 1- Codon, S. and Casanave, E.: Histological study of the salivary glands in *Zaedyus pichiy* (Mammalia, Xenarthra, Dasypodidae). *Int. J Morphol.*; 23(1):19-24, 2005.
- 2- Nezu, A., Tanimura, A., Morita, T., Irie, K., Yajima, T. and Tojyo, Y.: Evidence that zymogen granules do not function as an intracellular Ca<sup>2+</sup> store for the generation of the Ca<sup>2+</sup> signal in rat parotid acinar cells. *Biochem. J.*; 363:59-66, 2002.
- 3- Chen, L., Yang, Z., Chen, W., Lin, J., Zhang, M. and Yang, X.: Attenuated acute salivary alpha-amylase responses to gustatory stimulation with citric acid in thin children. *Br. J Nutr.*; 113:1078-1085, 2015.
- 4- Imai, A., Yoshie, S., Nashida, T., Shimomura, H. and Fukuda, M.: The small GTPase Rab27B regulates amylase release from rat parotid acinar cells. *Journal of Cell Science*; 117:1945-1953, 2004.
- 5- Faust, F., Gomez-Lazaro, M., Borta, H., Agricola, B. and Schrader, M.: Rab8 is involved in zymogen granule formation in pancreatic acinar AR42J cells. *Journal compilation*; 9:964-979, 2008.
- 6- Wennerberg, K., Rossman, K. and Der, C.: The Ras superfamily at a glance. *Journal of Cell Science*; 118:843-846, 2005.
- 7- Fukuda, M.: Regulation of secretory vesicle traffic by Rab small GTPases. *Cell. Mol. Life Sci.*; 65:2801-2813, 2008.
- 8- Rindler, M., Xu, C., Gumper, I., Smith, N. and Neubert, T.: Proteomic analysis of pancreatic zymogen granules: identification of new granule proteins. *J Proteome Res.*; 6:2978-2992, 2007.
- 9- Aframian, D. and Palmon, A.: Current status of the development of an artificial salivary gland. *Tissue Eng. Part B Rev.*; 14:187-198, 2008.
- 10- Napenas, J., Brennan, M. and Fox, P.: Diagnosis and treatment of xerostomia (dry mouth). *Odontology*; 97:76-83, 2009.
- 11- Ship, J., Pillemer, S. and Baum, B.: Xerostomia and the geriatric patient. *J Am. Geriatr. Soc.*; 50:535-543, 2002.
- 12- Jellema, A., Slotman, B., Doornaert, P., Leemans, C. and Langendijk, J.: Impact of radiation-induced xerostomia on quality of life after primary radiotherapy among patients with head and neck cancer. *Int. J Radiat. Oncol. Biol. Phys.*; 69:751-760, 2007.
- 13- Coppes, R. and Stokman, M.: Stem cells and the repair of radiation-induced salivary gland damage. *Oral Diseases*; 17(2):143-153, 2011.
- 14- Granero-Moltó, F., Weis, J. and Miga, M.: Regenerative effects of transplanted mesenchymal stem cells in fracture healing. *Stem Cells*; 8(27):1887-1898, 2009.
- 15- Lin, C., Chang, F. and Chen, C.: Cell therapy for salivary gland regeneration. *J Dent. Res.*; 90:341-346, 2011.
- 16- Abdel Aziz, M., Atta, H., Mahfouz, S., Fouad, H., Roshdy, N., Ahmed, H., Rashed, L., Sabry, D., Hassouna, A. and Hasan, N.: Therapeutic potential of bone marrow-derived mesenchymal stem cells on experimental liver fibrosis. *Clin. Biochem.*; 40(12):893-899, 2007.

- 17- Fikry, H., Abdel Gawad, S. and Baher, W.: Therapeutic potential of bone marrow-derived mesenchymal stem cells on experimental liver injury induced by *Schistosoma mansoni*: a histological Study. *Int. J Stem Cells*; 9(1):96-106, 2016.
- 18- Kawakami, M., Ishikawa, H., Tanaka, A. and Mataga, I.: Induction and differentiation of adipose-derived stem cells from human buccal fat pads into salivary gland cells. *Human Cell*; 29:101–110, 2016.
- 19- Park, E., Dodds, J. and Smith, N.: Dose comparison of ultrasonic transdermal insulin delivery to subcutaneous insulin injection. *Int. J Nanomedicine*; 3(3):335–341, 2008.
- 20- Matosz, B., Dezdrobotu, C., Martonos, C., Luca, V., Bogdan, S. and Damian, A.: Major salivary glands topography in rats and their relation with the surrounding anatomical tissues. *Sci. Works Series C Vet. Med.*; 62(2):38-43, 2016.
- 21- Kathleen, R., Corning, P., Mulder, G., Luo, Y. and White, W.: Principles of rodent surgery for the new surgeon. *J Vis. Exp.*; 47:1-4, 2011.
- 22- Zhao, L., Yin, R., Wei, B., Li, Q., Jiang, Z., Chen, X. and Bi, K.: Comparative pharmacokinetics of cefuroxime lysine after single intravenous, intraperitoneal, and intramuscular administration to rats. *Acta Pharm. Sinica*; 33:1348–1352, 2012.
- 23- Hasani, A., Soljakova, M., Jakupi, M. and Ustalar-Ozgen, S.: Preemptive analgesic effects of midazolam and diclofenac in rat model. *Bosnian J Basic Med. Sci.*; 11(2):113-118, 2011.
- 24- Shredah, M. and El-Sakhawy, M.: Immunohistochemical expression of activated caspase-3 in the parotid salivary glands of rats after long administration of *Myristica fragrans*. *Int. J Adv. Res.*; 2(12):493-499, 2014.
- 25- Ramadan, E., Hegab, A., Hussein, Y. and Abdul Rahman, M.: Postnatal developmental changes of the parotid gland in albino rats: histological, immunohistochemical and morphometric study. *British J Sci.*; 11(2):1-15, 2014.
- 26- Bahamondes, V., Albornoz, A., Aguilera, S., Alliende, C., Molina, C., Castro, I., Urzúa, U., Quest, A., Barrera, M., González, S., Sánchez, M., Härtel, S., Hermoso, M., Leyton, C. and González, M.: Changes in Rab3D expression and distribution in the acini of Sjogren's syndrome patients are associated with loss of cell polarity and secretory dysfunction. *Arthritis and Rheum.*; 63(10):3126–3135, 2011.
- 27- Raffaniello, R., Lin, J., Wang, F. and Raufman, J.: Expression of Rab3D in dispersed chief cells from guinea pig stomach. *Biochimica et Biophysica Acta*; 1311(2):111-116, 1996.
- 28- Pfaffl, M.: A new mathematical model for relative quantification in real-time RT-PCR. *Nucleic Acids Res.*; 29:2003-2007, 2001.
- 29- Reaper, P., di Fagagna, F. and Jackson, S.: Activation of the DNA damage response by telomere attrition: a passage to cellular senescence. *Cell Cycle*; 3:543-546, 2004.
- 30- Frisard, M. and Ravussin, E.: Energy metabolism and oxidative stress: impact on the metabolic syndrome and the aging process. *Endocrine*; 29(1):27–32, 2006.
- 31- BhatiaDey, N., Kanherkar, R., Stair, S., Makarev, E. and Csoka, A.: Cellular senescence as the causal nexus of aging. *Front. Genet.*; 7(13):1-14, 2016.
- 32- Iorgulescu, G.: Saliva between normal and pathological. Important factors in determining systemic and oral health. *Journal of Medicine and Life*; 2(3):303-307, 2009.
- 33- Garbowska, M., Lukaszuk, B., Miklosz, A., Wroblewski, I., Kurek, K., Ostrowska, L., Chabowski, A., Zendzian-Piotrowska, M. and Zalewska, A.: Sphingolipids metabolism in the salivary glands of rats with obesity and streptozotocin induced diabetes. *J Cell Physiol.*; 232:2766–2775, 2017.
- 34- Tsuboi, T. and Fukuda, M.: Rab3A and Rab27A cooperatively regulate the docking step of dense-core vesicle exocytosis in PC12 cells. *J Cell Sci.*; 119: 2196–2203, 2006.
- 35- Merrins, M. and Stuenkel, E.: Kinetics of Rab27a-dependent actions on Vesicle docking and priming in pancreatic beta-cells. *J Physiol.*; 586:5367–5381, 2008.
- 36- Rajaniello, R., Lin, J., Schwimmer, R. and Ojakian, G.: Expression and localization of Rab3D in rat parotid gland. *Biochimica et Biophysica Acta*; 1450:352-363, 1999.
- 37- Yoo, C., Vines, J., Alexander, G., Murdock, K., Hwang, P. and Jun, H.: Adult stem cells and tissue engineering strategies for salivary gland regeneration: a review. *Biomaterials Research*; 18(9):1-12, 2014.
- 38- Lim, J., Yi, T., Choi, J., Jang, Y., Lee, S., Kim, H., Song, S. and Kim, Y.: Intraglandular transplantation of bone marrow-derived clonal mesenchymal stem cells for amelioration of post-irradiation salivary gland damage. *Oral Oncol.*; 49:136-143, 2013.

- 39- Bruna, F., Contador, D., Conget, P., Erranz, B., Sossa, C. and Arango-Rodríguez, M.: Regenerative potential of mesenchymal stromal cells: age-related changes. *Stem Cells Int.*; 2016:1-15, 2016.
- 40- Pringle, S., Van Os, R. and Coppes, R.: Concise review: Adult salivary gland stem cells and a potential therapy for xerostomia. *Stem Cells*; 31:613–619, 2013.
- 41- Mednieks, M., Szczepanski, A., Clark, B. and Hand, A.: Protein expression in salivary glands of rats with streptozotocin diabetes. *International Journal of Experimental Pathology*; 90:412–422, 2009.
- 42- Tamgadge, S., Tamgadge, A., Satheesan, E. and Modak, N.: Myoepithelial Cell – A Morphologic Diversity – A Review. *A Journal of Dentistry*; 4(1):1-10, 2013.
- 43- Igbokwe, C.: Ultrastructure of the parotid salivary gland in the greater cane rats (*Thryonomys swinderianus*). *Journal of Microscopy and Ultrastructure*; 126:1-8, 2017.
- 44- Chakrabarti, I., Basu, A. and Chosh, N.: Oncocytic lesion of parotid gland: a dilemma for cytopathologists. *Journal of Cytology*; 29:80-82, 2012.
- 45- Yasear, A., Sultan, A. and Elramli, A.: Premature age changes associated with cimetidine treatment: a histological study. *Australian Journal of Basic and Applied Sciences*; 7:85-92, 2013.
- 46- Enoki, N., Kiyoshima, T., Sakai, T., Kobayashi, I., Takahashi, K. and Terada, Y.: Age-dependent changes in cell proliferation and cell death in the periodontal tissue and the submandibular gland in mice: a comparison with other tissues and organs. *Journal of Molecular Histology*; 38(4):321–332, 2007.
- 47- Kroemer, G. and Levine, B.: Autophagic cell death: the story of a misnomer. *Nature Reviews Molecular Cell Biology*; 9(12):1004–1010, 2008.
- 48- Kontaxis, A., Zanarotti, U., Kainz, J. and Beham, A.: Diffuse hyperplastic oncocytosis of the parotid gland. *Laryngorhinootologie*; 83:185–188, 2004.
- 49- Terman, A., Kurz, T., Navratil, M., Arriaga, A. and Brunk, U.: Mitochondrial turnover and aging of long-lived postmitotic cells: the mitochondrial–lysosomal axis theory of aging. *Antioxid. Redox Signal.* 12(4):503–535, 2010.
- 50- Hagra, G., Soliman, M. and Kafafy, M.: Histological study on the effect of diazepam on parotid gland of adult male albino rat and the possible protective effect of pilocarpine. *Menoufia Medical Journal*; 24:41-58, 2011.
- 51- Tirapelli, L., Tirapelli, D. and Schimming, B.: Ultrastructural alterations of the parotid glands of rats submitted to experimental chronic alcoholism. *Revista Chilena de Anatomia*; 19:1-9, 2012.
- 52- Schrader, M.: Membrane targeting in secretion. *Subcellular Biochemistry*; 37: 391-421, 2004.
- 53- Witt, H., Apte, M., Keim, V. and Wilson, J.: Chronic pancreatitis: challenges and advances in pathogenesis, genetics, diagnosis, and therapy. *Gastroenterology*; 132(4):1557-1573, 2007.
- 54- Xu, J., Wang, D., Liu, D., Fan, Z., Zhang, H., Liu, O., Ding, G., Gao, R., Zhang, C., Ding, Y., Bromberg, J., Chen, W., Sun, L. and Wang, S.: Allogeneic mesenchymal stem cell treatment alleviates experimental and clinical Sjogren syndrome. *Blood*; 120:3142–3151, 2012.
- 55- Mikkelsen, R. and Wardman, P.: Biological chemistry of reactive oxygen and nitrogen and radiation-induced signal transduction mechanisms. *Oncogene*; 22:5734–5754, 2003.
- 56- Sumita, Y., Liu, Y., Khalili, S., Maria, O., Xia, D., Key, S., Cotrim, A., Mezey, E. and Tran, S.: Bone marrow-derived cells rescue salivary gland function in mice with head and neck irradiation. *Int. J Biochem. Cell Biol.*; 43:80–87, 2011.
- 57- Baer, P. and Geiger, H.: Mesenchymal stem cell interactions with growth factors on kidney repair. *Curr. Opin. Nephrol. Hypertens.*; 19:1-6, 2010.
- 58- Bai, X., Yan, Y. and Coleman, M.: Tracking long-term survival of intramyocardially delivered human adipose tissue-derived stem cells using bioluminescence imaging. *Mol. Imaging Biol.*; 13:633-645, 2011.
- 59- Liu, Z., Hu, G., Luo, X., Yin, B., Shu, B., Guan, J. and Jia, C.: Potential of bone marrow mesenchymal stem cells in rejuvenation of the aged skin of rats. *Biomedical Reports*; 6:279-284, 2017.
- 60- Quintanilha, L., Takami, T., Hirose, Y., Fujisawa, K., Murata, Y., Yamamoto, N., Goldenberg, R., Terai, S. and Sakaida, I.: Canine mesenchymal stem cells show antioxidant properties against thioacetamide-induced liver injury in vitro and in vivo. *Hepatology Research*; 44:206–217, 2014.
- 61- Aluri, H., Samizadeh, M., Edman, M., Hawley, D., Armaos, H., Janga, S., Meng, Z., Sendra, V., Hamrah, P., Kublin, C., Hamm-Alvarez, S. and Zoukhri, D.: Delivery of bone marrow-derived mesenchymal stem cells improves tear

- production in a mouse model of Sjogren's syndrome. *Stem Cells International*; 2017:1-10, 2017.
- 62- Mizushima, N., Levine, B., Cuervo, A. and Klionsky, D.: Autophagy fights disease through cellular self-digestion. *Nature*; 451:1069-1075, 2008.
- 63- Vellai, T., Takács-Vellai, K., Sass, M. and Klionsky, D.: The regulation of aging: does autophagy underlie longevity? *Trends Cell Biol.*; 19:487-94, 2009.
- 64-Tanguy, E., Carmon, O., Wang, Q., Jeandel, L., Chasserot-Golaz, S., Montero-Hadjadje, M. and Vitale, N.: Lipids implicated in the journey of a secretory granule: from biogenesis to fusion. *J Neurochem.*; 137(6):904-912, 2016.
- 65- Shah, F., Goossens, E., Atallah, N., Grimard, M., Kelley, M. and Fishel, M.: APE1/Ref-1 knockdown in pancreatic ductal adenocarcinoma – characterizing gene expression changes and identifying novel pathways using single-cell RNA sequencing. *Molecular Oncology*; 11:1711–1732, 2017.
- 66- Ngyen, D., Jones, A., Ojakian, G. and Raffaniello, R.: Rab3D redistribution and function in rat parotid acini. *J Cell. Phys.*; 197:400–408, 2003.
- 67- Hagen, C., Dent, K., Zeev-Ben-Mordehai, T., Grange, M., Bosse, J., Whittle, C., Klupp, B., Siebert, C., Vasishtan, D., Ba'uerlein, F., Cheleski, J., Werner, S., Guttmann, P., Rehbein, S., Henzler, K., Demmerle, J., Adler, B., Koszinowski, U., Schermelleh, L., Schneider, G., Enquist, L., Plitzko, J., Mettenleiter, T. and Grünwald, K.: Structural basis of vesicle formation at the inner nuclear membrane. *Cell*; 163:1692–1701, 2015.
- 68- Batista, T., Tomiyoshi, L., Dias, A., Roma, L., Módulo, C., Malki, L., Filho, E., Deminice, R., Jr, A., Cunha, D. and Rocha, E.: Age-dependent changes in rat lacrimal gland anti-oxidant and vesicular related protein expression profiles. *Molecular Vision*; 18:194-202, 2012.
- 69- Alao, J. and Sunnerhagen, P.: Rad3 and Sty1 function in *Schizosaccharomyces pombe*: an integrated response to DNA damage and environmental stress? *Molecular Microbiology*; 68(2):246–254, 2008.
- 70- Paliwal, S., Kakkar, A., Sharma, R., Airan, B. and Mohanty, S.: Differential reduction of reactive oxygen species by human tissue specific mesenchymal stem cells from different donors under oxidative stress. *J Biosci.*; 42(3):373–382, 2017.